D. W. Worthem, C. J. Altstetter,* I. M. Robertson,* and D. F. Socie**

Cyclic Deformation and Damage Structure in Inconel 718

REFERENCE Worthem, D. W., Altstetter, C. J., Robertson, I. M., and Socie, D. F., **Cyclic deformation and damage structure in Inconel 718,** *Biaxial and Multiaxial Fatigue*, EGF 3 (Edited by M. W. Brown and K. J. Miller), 1989, Mechanical Engineering Publications, London, pp. 131–143.

ABSTRACT To understand the cyclic softening and the crack initiation and propagation observed in Inconel 718 during low-cycle fatigue tests, the surface morphology and deformation microstructure, produced under different loading conditions, have been examined by scanning and transmission electron microscopy. The morphology and microstructure produced during room temperature low-cycle fatigue tests were compared using pure tension, pure torsion, and combined-proportional torsion and tension tests.

The fracture mode under the different loading conditions was transgranular. In the early stages of the life, near surface, semi-elliptical, part-through-thickness cracks which had nucleated at inclusions, propagated in a stepped and faceted manner along intense deformation bands. Late in the fatigue life, the fracture mode changed to ductile microvoid coalescence. This change coincided with the crack-propagation mode transition from a Stage I to a Stage II type.

The deformation microstructure produced by each loading condition was identical. It consisted of a regularly spaced array of deformation bands. Within the deformation bands dense tangles of dislocations were observed, but there was no evidence of the γ' and γ'' precipitates that contribute to the strength of this material. Outside the bands there was no evidence of dislocation pairs existing, but partial dislocations were observed. The macroscopic effect of cyclic softening during low-cycle fatigue tests is, therefore, a consequence of the lower stress required to move dislocations along 'precipitate-free' deformation bands.

Introduction

The uniaxial low-cycle fatigue response of a precipitate-hardened alloy, Inconel 718, has been the subject of several studies (**1–4**). These studies have investigated macroscopic stress–strain response, cyclic deformation structures, and fracture behaviour, at temperatures between 300 and 922 K.

Previous uniaxial tests demonstrated that the cyclic deformation response could be separated into two regimes, cyclic hardening and cyclic softening. The cyclic hardening regime occurs within the first one hundred cycles and has been attributed to the interaction between dislocations and precipitates. The softening regime extends throughout the remainder of the life and is attributed to the reduced stress required to move dislocations along the easy glide paths established by the dislocations progressively shearing the γ' and γ'' precipitates. The restriction of dislocation motion to paths where precipitates have been

* Materials Research Laboratory, University of Illinois at Urbana-Champaign, 104 S. Goodwin, Urbana, IL 61801, USA.

sheared produces a deformation band. Fournier and Pineau (2) claim that all deformation bands are twins. The mechanism by which dislocations shear the precipitates is not well understood. The passage of a single, perfect or dissociated, dislocation through a precipitate will produce an unstable, high-energy fault in the precipitate. The fault will be eliminated by the passage of a second dislocation. Oblak *et al.* (5) suggested that the formation of a high-energy fault would be eliminated if the dislocations passed through the precipitates in pairs. They observed dislocation pairs in Inconel 718 that had been deformed monotonically.

Fournier and Pineau (2) observed the initiation of microcracks along the slip band matrix interface at about 70 per cent of the total life. The crack propagation mode changed from a Stage I to a Stage II type after propagating a few grains beneath the surface. The propagation mode was transgranular and the fracture surface striated. Clavel and Pineau (4) reported that the deformation structure at the crack tip of a standard fatigue crack growth specimen, at near-threshold crack propagation rates, was similar to that in a low-cycle fatigue specimen. Additionally, the fracture surface in the fatigue crack growth specimen had smooth and planar areas and facets identical to the fracture surface in the Stage I regime of a low-cycle fatigue specimen. This crystallographic morphology was attributed to decohesion along the twin bands. At higher crack propagation rates the fracture surface was striated with a more homogeneous (fine slip) deformation structure. For near-threshold crack propagation rates, Clavel and Pineau created a life prediction model based on the idea that fatigue crack propagation is a low-cycle fatigue damage process restricted to the neighbourhood of the crack tip (6).

Previous studies on Inconel 718 have used uniaxial loadings. In many applications, components are subjected to multiaxial states of stress and strain. Therefore, a better understanding of the material's response to in-service conditions can be obtained by performing multiaxial low-cycle fatigue experiments. This paper and the one presented in these proceedings by Socie *et al.* (7), respectively, describe the microscopic and macroscopic results of experiments on thin-walled (2mm), cylindrical (29 mm outside diameter) tubes subjected to biaxial total strain control tests at room temperature. The cyclic deformation structure, fracture surface morphology, and physical crack behaviour are reported to explain the cyclic stress–strain response and overall failure behaviour.

Experimental procedure

The material used in this investigation was Inconel 718 which complied with Aerospace Material Specification, AMS 5663D. This material is strengthened by both solid solution and precipitation hardening (5)(8)(9). The primary strengthening precipitate is disc-shaped with an orientation with the matrix of (001) $\gamma'' \parallel \{001\}\ \gamma$ and $[200]\gamma'' \parallel \langle 100\rangle\gamma$ (3 variants) (2)(8). The precipitates were about 30 nm in diameter and about 6 nm in thickness. These precipitates have

a DO_{22} type bct structure based on Ni_3Nb and provide coherency strengthening (**5**)(**8**)(**9**). The γ' precipitate, which is spherical with a 20 nm diameter, has a $L1_2$ fcc structure of a general stoichiometry of Ni_3 (Al, Ti) and provides order and coherency strengthening (**5**)(**8**)(**9**). The strengthening due to the γ' precipitates is of secondary importance since it accounts for only 4 per cent of the volume compared to 15 per cent for the γ''. Large carbide and nitride precipitates are found throughout the material.

Fatigue tests to failure were carried out at room temperature on an MTS tension–torsion facility. Failure was defined as that cycle when the load dropped 10 per cent between successive cycles. Loadings were pure torsion, pure tension, and combined proportional tension–torsion. For each loading condition, a series of tests was conducted at an effective strain amplitude (von Mises) of 1.0 per cent and another at 0.5 per cent. At the higher strain amplitude, about 50 per cent of the total strain is plastic and at the lower, 10 per cent is plastic. The tests at each amplitude were conducted at two strain ratios, $R_{\bar{\varepsilon}} = -1$ and 0. Test frequencies varied from 0.075 to 0.5 Hz, which is relatively low and is not considered a variable in these experiments. Surface replication to monitor crack formation and propagation was performed at approximately every 5–10% per cent of the estimated fatigue life of each specimen.

Results and discussion

The macroscopic deformation and crack growth results are described in detail in the papers by Socie *et al.* (**7**)(**10**) and not repeated here. Of major relevance to this paper is the result that, for the three loading conditions, at the same effective strain amplitude, the material hardens during the first few cycles and then softens for the remainder of the life. This result is consistent with the observations made in uniaxial tests (**1**)–(**4**). This result will be correlated with the microstructure described in the following sections.

For the three loading conditions investigated, a high density of transgranular microcracks formed on the surface early in the life (*circa* 10 per cent) because of the homogeneous nominal plastic strains. A microcrack is on the order of the grain size (30 microns). These fatigue cracks initiated at both slip band intersections with the surface and at inclusions (carbides and nitrides) at the surface or immediately below the surface either by fracture or debonding of the inclusions. This initiation occurred on planes of maximum shear strain amplitude. It was noted that the main failure cracks were generally formed at inclusions. The cracks propagated by a combination of crack tip advance and by linkage with nearby cracks and microcracks. Microcracks were continually formed throughout the life.

For the pure tensile case, two systems of microcracks develop at the surface, either at a positive or negative angle between the surface trace and the circumferential direction on the surface. The failure crack develops by the advance and linkage of these microcracks; by about half of the life of the specimen one crack, the failure crack, dominates. Figure 1(a) is a scanning

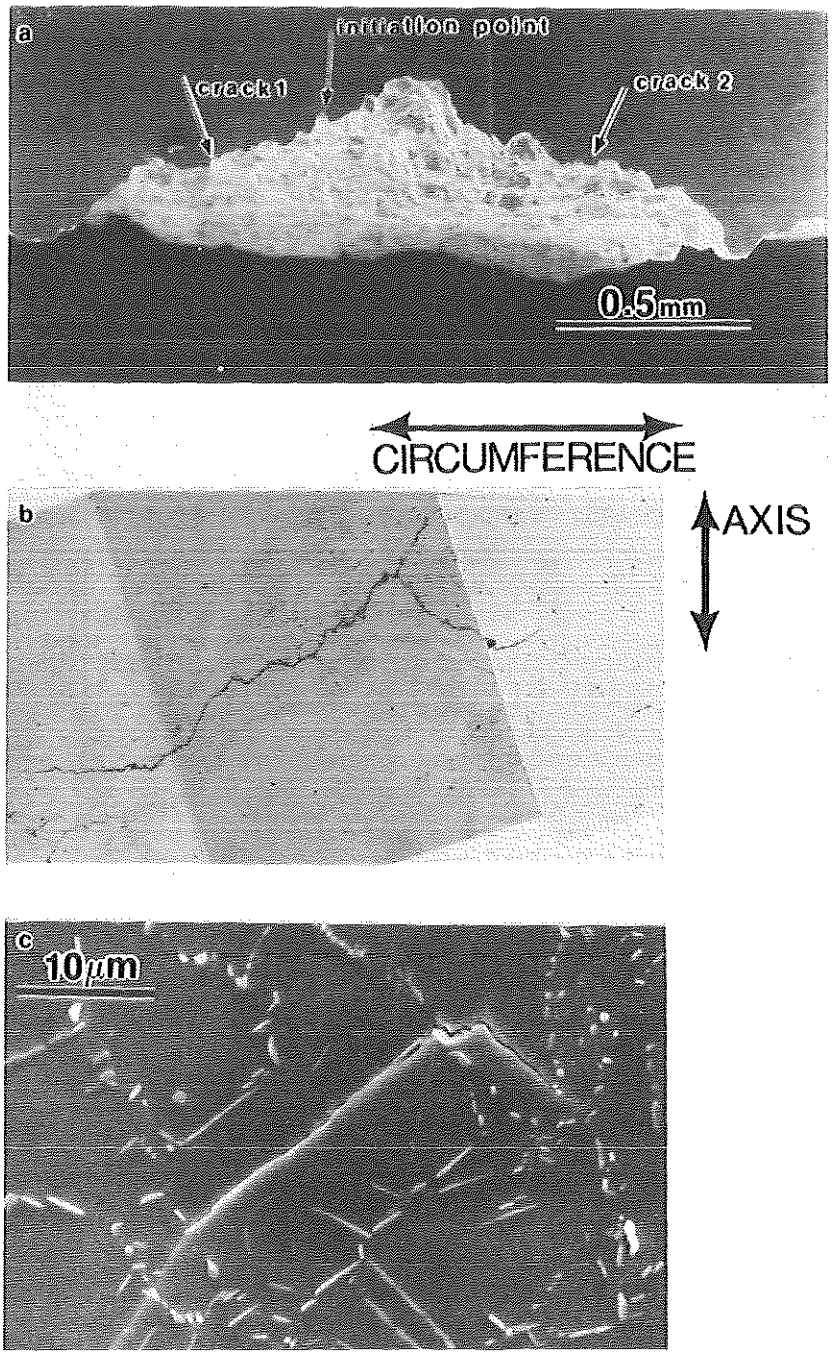

Fig 1 Crack propagation for a sample loaded in pure tension ($\Delta\bar{\varepsilon}/2 = 1.0$ per cent, $R_\varepsilon = 0$). (a) A radial view of macroscopic crack propagation of failure crack ($N_f = 936$), (b) plastic replica of the crack in (a) at $N = 900$, and (c) microcrack propagation on an etched surface

electron micrograph of one failure crack which formed by the propagation and linkage of two microcracks (labelled '1' and '2'). On the surface these microcracks are at an angle of approximately ±30 degrees to the circumferential direction. For all the tensile cases, the angle of the microcracks with respect to the circumferential direction varied from 0 to ±45 degrees with the average being about ±35 degrees. These angles were measured from plastic replicas (such as Fig. 1(b)) which allow angles to be accurately determined. This average angle can be rationalized by considering the planes with equal shear strains into and out of and along the surface. For axisymmetric deformation all possible maximum shear planes form a cone at 45 degrees to the tensile axis. Because of the sample geometry, the planes with equal shear components into and out of and along the surface can be shown to be at ±35 degrees to the circumferential direction. For this angle of ±35 degrees there would be an angle into the surface of ±30 degrees. Stereomicroscopy of the fracture surface of the sample of Fig. 1(a) and 1(b) gave an angle into the surface of about ±20 degrees; optical microscopy of cross-sectional cuts of the crack gave the crack angle into the surface of about ±30 degrees (**11**). Due to inaccuracies associated with stereomicroscopic calculations, the discrepancy between the angles measured by the different techniques is not believed to be significant.

A close examination of Fig. 1(a) shows that the fracture surface near the sample surface is jagged. These jagged features arise from the crack changing direction to propagate along the favoured slip plane in each grain closest to the applied maximum shear strain direction. This tendency for the crack direction to change abruptly on crossing a grain boundary is more evident in Fig. 1(c) which shows a micrograph of the etched surface. Although on a fine scale the crack direction changes, macroscopically the direction is constant.

At approximately half the fatigue life in tension loading, the failure crack which initially propagated on the maximum shear strain planes changed direction and propagated normal to the maximum principal strain direction. This change in crack propagation direction is the transition from Stage I to Stage II type propagation.

For the samples tested in pure torsion, cracks initiate and propagate to failure along the two unique planes of maximum shear strain amplitude; one plane has a normal parallel to the specimen axis and the other a normal perpendicular to the specimen axis and in the circumferential direction; both planes are perpendicular to the specimen surface. Both have the shear strain parallel to the specimen surface. As shown in Fig. 2(a) the failure crack favoured the direction parallel to the specimen axis although at some points (marked A and B in the figure) the crack propagated in the direction perpendicular to the specimen axis. This favouring of one maximum shear strain plane over another is thought, in this case, to be an artifact of the specimen geometry. In contrast to the samples loaded in tension, cracks in torsion propagated through grains apparently without regard to favoured slip planes (see Fig. 2(b)). Furthermore, the crack lengths at incipient failure are different in torsion and tension samples. In torsion, many cracks are tens of millimetres in length,

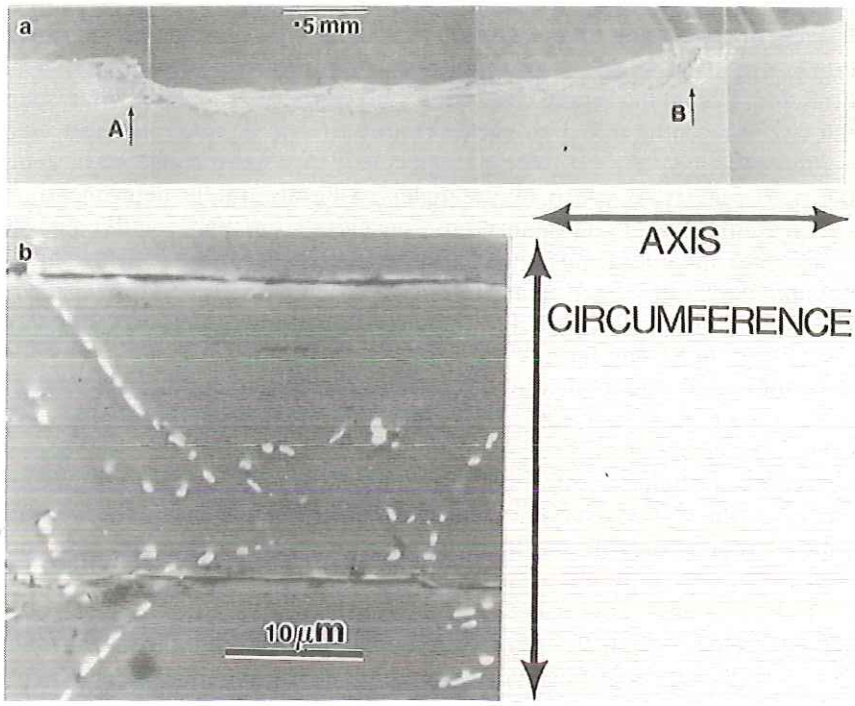

Fig 2 Crack propagation for a sample loaded in pure torsion ($\Delta\bar{\varepsilon}/2 = 0.5$ per cent, $R_{\bar{\varepsilon}} = -1$). (a) A radial view of macroscopic crack propagation, and (b) microcrack propagation on an etched surface

and the failure crack develops by linkage between these large cracks. In contrast, in tension the maximum length of the failure crack at incipient failure is about 2 mm and only a few cracks approach this size.

The behaviour of cracks in the combined tension–torsion case was intermediate between the tensile and torsional cases. That is, the cracks initiated and propagated on both maximum shear strain planes, changing to the plane perpendicular to the maximum principal strain very late in the life. The maximum shear strain planes (two unique planes) under this loading condition intersect the specimen surface at 20 degrees and −70 degrees to the specimen axis and both are perpendicular to the specimen surface, and, similar to the torsion case, the cracks favour the 20 degree plane.

The fracture surface for a pure tension case is shown in the micrographs of Fig. 3(a), (b), (c). The micrographs of Fig. 3(a) and (b) indicate that near the specimen surface the fracture surface is crystallographic with the crack propagating along deformation or slip bands that were produced during the cyclic plastic straining. The spacing between bands is quite regular at about 0.7 microns. Further into the surface the crack propagation mode changes to

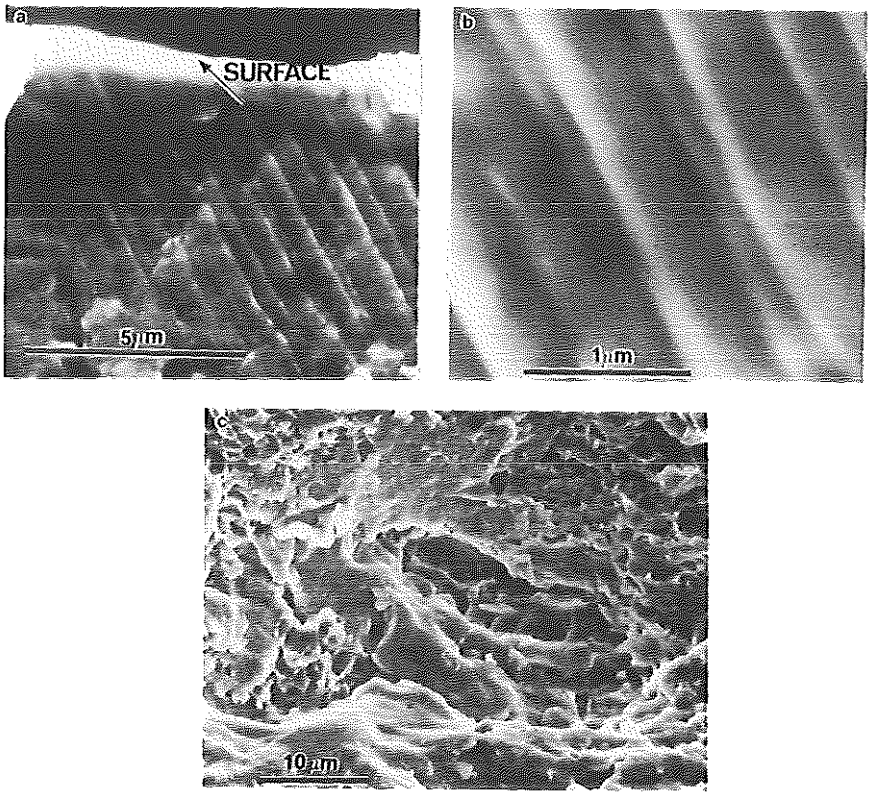

Fig 3 Fracture surface near the specimen surface for a sample loaded in pure tension. (a) At high magnification, (b) at very high magnification, (c) microvoids on fracture surface deeper into the specimen

ductile microvoid coalescence (Fig. 3(c)). The depth at which microvoid coalescence starts approximately coincides with the depth at which the crack propagation mode changes from Stage I to Stage II. This result suggests that the transition in crack propagation mode is associated with a change in the fatigue fracture mechanism. For the torsion case, the fracture surface morphology is identical to that observed in tension, except that the voids are elongated, as would be expected for pure applied shear. This result indicates that although there is no change in the crack propagation direction, a Stage I to Stage II type transition does occur in torsion. Also the torsion case has more crack rubbing due to the higher shear deformations with no normal displacements of the crack surfaces.

The deformation microstructure produced by different loading conditions was investigated by transmission electron microscopy. The thin foils for electron microscopy were prepared from discs cut at random from the centre of

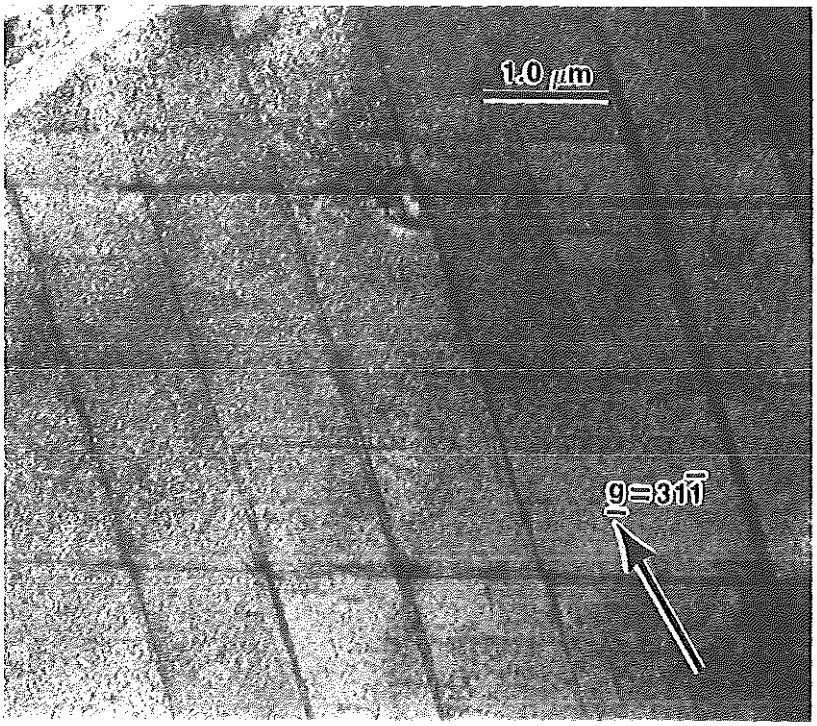

Fig 4 Bright-field micrograph showing coarse arrays of deformation bands in {111} planes. The sample was loaded in pure tension ($\Delta\bar{\varepsilon}/2 = 1.0$ per cent, $R_\varepsilon = 0$). The beam direction was B = [011]

the gauge length close to the surface. These discs were jet polished to perforation in a 10 per cent solution of sulphuric acid in methanol with 10 per cent as much butyl cellusolve as methanol. Polishing was performed at a temperature between 258 and 268 K using a potential of 38 V.

The microstructure was similar for all loading conditions. That is, the microstructure consisted of a well developed coarse array of planar deformation bands on {111} planes. One or two planes were activated in individual grains. A typical microstructure is shown in Fig. 4. The average spacing between the deformation bands was relatively uniform (0.5–1.0 microns) throughout the grain. Note that this distance corresponds to the spacing of the surface steps observed in Fig. 3(b). A few deformation bands appeared to be microtwins; this is in contrast to Fournier and Pineau's results (2) where they claimed that all deformation bands were twins. The deformation bands were not observed in undeformed material.

Details of the precipitate morphology in the deformation band and matrix were investigated by using the precipitate diffraction spots to image the γ' and γ'' precipitates. The micrograph in Fig. 5 was taken using a precipitate

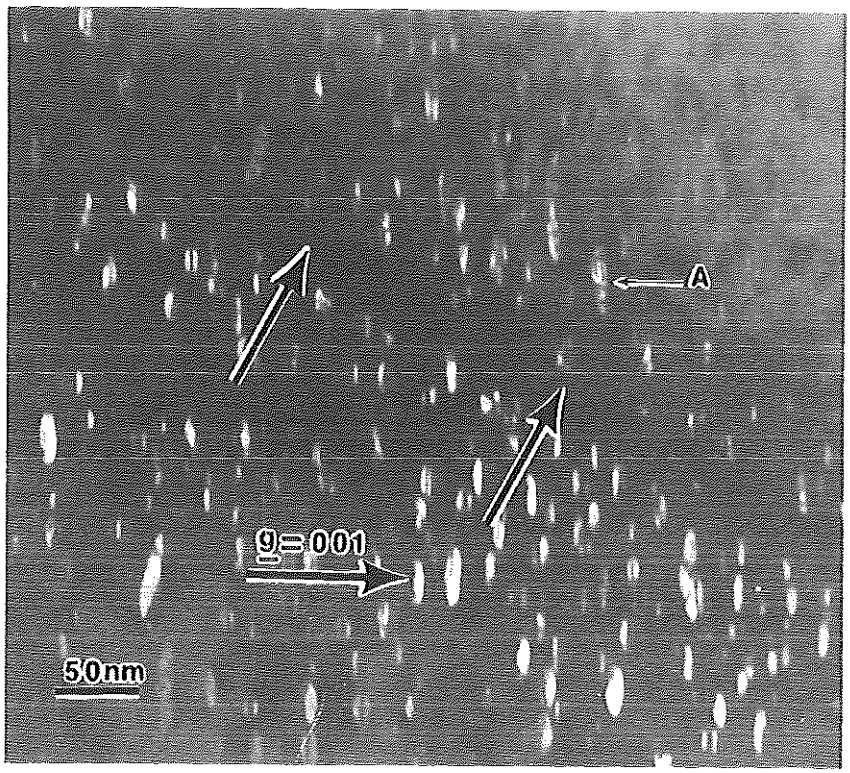

Fig 5 Dark-field micrograph showing a deformation band denuded of precipitates. A faulted precipitate is arrowed (A). The diffracting vector is $g = [001]$ which images both precipitates and the beam direction is $B = [011]$. This sample was loaded in pure torsion ($\Delta\bar{\epsilon}/2 = 1.0$ per cent, $R_\epsilon = 0$)

diffraction spot which images both the γ' and γ'' precipitates. A band, the deformation band, can be seen to be devoid of precipitates. This indicates that there are no visible precipitates remaining within the deformation band. The band width which was determined by tilting the bands edge-on was approximately 30 nm wide, which corresponds to the diameter of the precipitates.

Examination of the dislocation structure within the deformation bands and the matrix is complicated by the large coherency strain associated with the precipitates and also the large density of precipitates (5)(8). However, by using the weak-beam imaging technique, dislocations were observed within the deformation bands and the matrix. As shown in Fig. 6, the dislocation structure within the deformation bands consists of complex tangles of dislocations which appear to be arranged in cellular networks (arrow). Some of the dislocations in the matrix are observed to be in the form of partial dislocations; an example is labelled A in Fig. 6. There was no evidence for perfect dislocation pairs forming; the distance between dislocations on the same slip plane was several

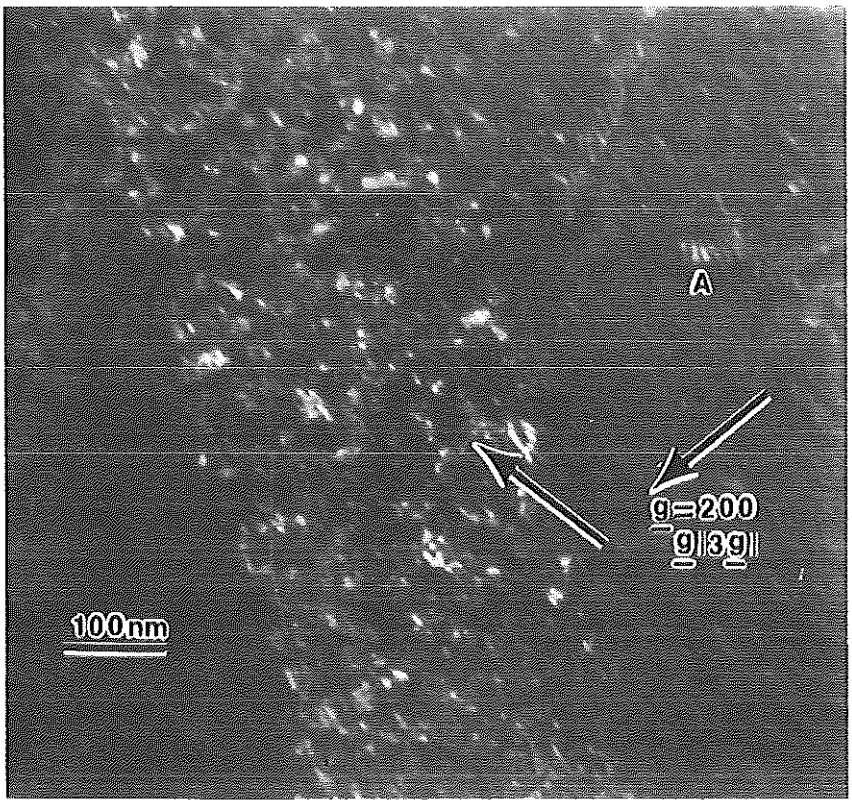

Fig 6 Weak-beam micrograph showing the complex cellular dislocation networks (arrow) within a deformation band. An example of a stacking fault bounded by partial dislocations is labelled 'A'. The sample was loaded in pure tension ($\Delta\bar{\varepsilon}/2 = 1.0$ per cent, $R_\varepsilon = 0$)

precipitate diameters. Although there is no direct evidence that partial dislocations shear the precipitates, it has been shown that they exist in this material. There is also some evidence for faulted precipitates existing in the matrix; an example of a faulted precipitate is shown (labelled A) in Fig. 5.

Crack propagation, at least early in the life, is along the deformation bands which is in accord with the near surface fractography and plastic replication results. An example of this is shown in Fig. 7, where deformation slip bands can be seen running parallel to the fracture surface. 'Jumping' between parallel bands is also observed. It is believed that the crack in Fig. 7 is caused by the fatigue process rather than by handling, because such cracks were not found in foils prepared under conditions where they are not expected to exist: for example, in the bulk of a sample subjected to low-cycle fatigue for only 2 per cent of the life where the deformation bands are almost fully formed and cracks have not initiated to a great extent at the surface, no cracks were observed.

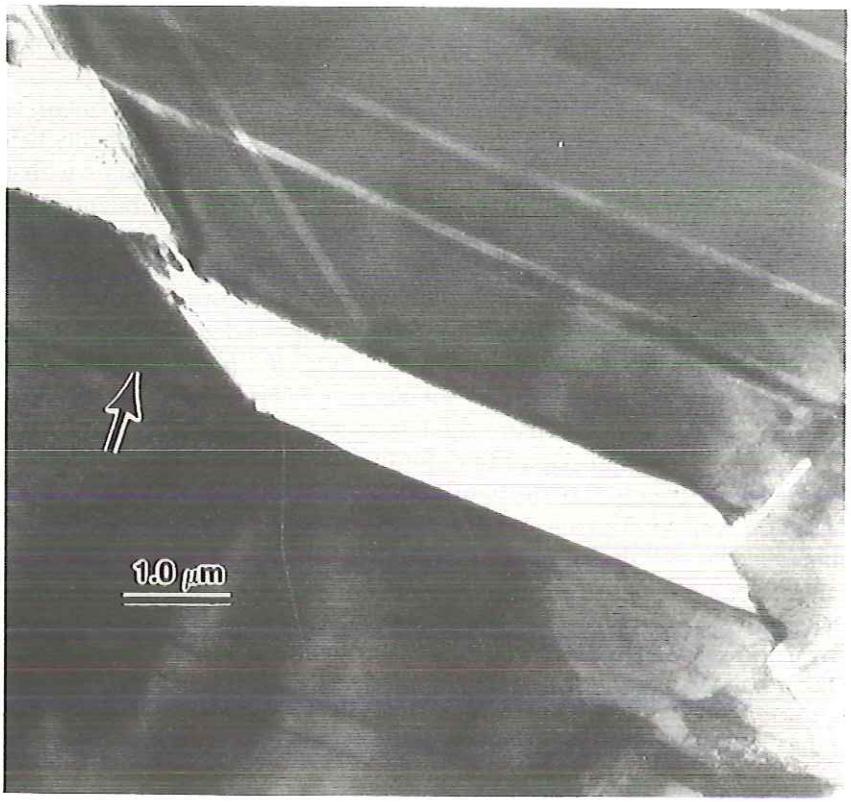

Fig 7 Bright-field electron micrograph showing a microcrack propagating along a deformation band (arrow). This sample was loaded in combined tension–torsion ($\Delta\bar{\varepsilon}/2 = 1.0$ per cent, $R_{\bar{\varepsilon}} = 0$)

Furthermore, foils of deformed material strained *in situ* in the microscope experienced crack propagation along a band.

Summary

Macroscopic cyclic softening occurs under multiaxial loading conditions. The micromechanism responsible for this softening is identical to that responsible for cyclic softening observed under uniaxial loading. That is, the passage of dislocations through the precipitates leads to the development of an easy slip path. Continued shearing of the precipitates along this slip path leads to the formation of the deformation band. Within these bands the precipitates are either submicroscopic (<1 nm) or have returned to solid solution. The dislocation (partial, single perfect or pairs of perfect dislocations) responsible for shearing the particles still remains to be determined, although partial dislocations have been observed in the matrix. There was no evidence for the

dislocations existing in pairs in either the matrix or the deformation bands. The mechanisms of precipitate shearing and the formation of the deformation bands is being investigated further.

Microcrack initiation occurs throughout the life. Two sites for microcrack initiation were identified; carbide/nitride inclusions at or immediately below the specimen surface and intersections of the deformation bands with the specimen surface. Initiation at inclusions is probably a consequence of the stress build-up by dislocations impeded by inclusions, either fracturing the inclusions or debonding them from the matrix. Initiation at the deformation bands appears to be the result of an intrusion–extrusion process.

Stage I type crack propagation is localized along the deformation bands and can occur along more than one plane in a grain by 'jumping' or turning to propagate along the bands on different planes in the grain. This explains why a crack in a torsional specimen propagates in the applied maximum shear strain plane without apparent regard to deformation bands in an individual grain. Crack advance is a result of the interaction of the dislocation networks with the crack. The transition to Stage II may occur when the cracks are large enough relative to the wall thickness to be subjected to large crack-opening displacements in tension and crack displacements in torsion to initiate and grow microvoids ahead of the crack. The mechanisms of crack initiation and propagation is being investigated further.

Qualitatively, there is no effect of the strain amplitude or the strain ratio (strain amplitudes were both in the low-cycle fatigue range). Quantitatively, the life decreases with the strain amplitude according to a modified Coffin–Manson relationship which accounts for the mean stress experienced in the $R_{\tilde{\varepsilon}} = 0$ samples (**10**). The effect of the mean stress is especially prominent in the tensile case where the life drops by about 25 per cent for $\Delta\bar{\varepsilon}/2 = 1.0$ per cent and 50 per cent for $\Delta\bar{\varepsilon}/2 = 0.5$ per cent for $R_{\tilde{\varepsilon}} = 0$ compared to $R_{\tilde{\varepsilon}} = 1$ (the smaller strain amplitude specimens experience less mean stress relaxation). For the other loading modes the effect on life is much less. Also, the density of cracks over 0.1 mm in length decreases as the maximum shear strain amplitude decreases and as $R_{\tilde{\varepsilon}}$ changes from -1 to 0 (**13**). The above probably indicates the effect of hydrostatic stress and normal plastic strain in nucleating and growing microvoids ahead of the crack tip.

Acknowledgements

This work was supported by the DOE Division of Material Science through contract DEAC02–76ER01198.

References

(1) MERRICK, H. F. (1974) The low cycle fatigue of three wrought nickel-base alloys, *Met. Trans*, **5**, 891–897.

(2) FOURNIER, D. and PINEAU, A. (1977) Low cycle fatigue behavior of Inconel 718 at 298°K and 823°K, *Met. Trans*, **8A**, 1095–1105.

(3) SANDERS, T. H., Jr, FRISHMUTH, R. E., and EMBLEY, F. T. (1981) Temperature dependent deformation mechanisms of alloy 718 in low cycle fatigue, *Met. Trans*, **12A**, 1003–1010.

(4) CLAVEL, M. and PINEAU, A. (1982) Fatigue behaviour of two nickel-base alloys: I. Experimental results on low cycle fatigue, fatigue crack propagation, and substructures, *Mater. Sci. Engng*, **55**, 157–171.

(5) OBLAK, J. M., PAULONIS, D. F., and DUVALL, D. S. (1974) Coherency strengthening in nickel-base alloys hardened by DO_{22} γ'' precipitates, *Met. Trans*, **5**, 143–153.

(6) CLAVEL, M. and PINEAU, A. (1982) Fatigue behaviour of two nickel-base alloys: II. Physical modelling of the fatigue crack propagation process, *Mater. Sci. Engng*, **55**, 173–180.

(7) SOCIE, D. F., KURATH, P., and KOCH, J. (1988) A multiaxial fatigue damage parameter, *Biaxial and Multiaxial Fatigue*, ECF 3 (Edited by BROWN, M. W. and MILLER, K. J.), Mechanical Engineering Publications, London, pp. 537–552. *This volume*.

(8) PAULONIS, D. F., OBLAK, J. M., and DUVALL, D. S. (1969) Precipitation in nickel-base alloy 718, *Trans ASM*, **62**, 611–622.

(9) CHATURVEDI, M. C. and HAN, Y.-F. (1973) Strengthening mechanisms in Inconel 718 superalloy, *Metals Sci.*, **17**, 145–149.

(10) SOCIE, D. F., WAILL, L. A., and DITTMER, D. F. (1985) *Biaxial fatigue of Inconel 718 including mean stress effects, ASTM STP 853.*

(11) BEER, T. A. (1983) *Crack shapes during biaxial fatigue*, MS thesis, Department of Mechanical and Industrial Engineering, University of Illinois at Urbana-Champaign.

(12) WAILL, L. E. (1983) Crack observations in biaxial fatigue, Report No. 108, Design and Materials Division, Department of Mechanical and Industrial Engineering, University of Illinois at Urbana-Champaign.